Limits on primordial non-Gaussianity from Minkowski Functionals of the WMAP temperature anisotropies

C Hikage, T Matsubara, P Coles, M Liguori, F K Hansen, S Matarrese

Publication date
01-09-2008

Published in
Monthly Notices of the Royal Astronomical Society

Link to external publisher version
https://doi.org/10.1111/j.1365-2966.2008.13674.x

Limits on primordial non-Gaussianity from Minkowski Functionals of the WMAP temperature anisotropies

Article (Unspecified)

Hikage, C, Matsubara, T, Coles, P, Liguori, M, Hansen, F K and Matarrese, S (2008) Limits on primordial non-Gaussianity from Minkowski Functionals of the WMAP temperature anisotropies. Monthly Notices of the Royal Astronomical Society, 389 (3). pp. 1439-1446. ISSN 0035-8711

Mon. Not. R. Astron. Soc. **389,** 1439–1446 (2008) doi:10.1111/j.1365-2966.2008.13674.x

Limits on primordial non-Gaussianity from Minkowski Functionals of the *WMAP* temperature anisotropies

C. Hikage,[1,2]★ T. Matsubara,[3] P. Coles,[2] M. Liguori,[4] F. K. Hansen[5] and S. Matarrese[6,7]

[1]*School of Physics and Astronomy, University of Nottingham, University Park, Nottingham NG7 2RD*
[2]*School of Physics and Astronomy, Cardiff University, Queens Buildings, 5, The Parade, Cardiff CF24 3AA*
[3]*Department of Physics and Astrophysics, Nagoya University, Chikusa, Nagoya 464-8602, Japan*
[4]*Department of Applied Mathematics and Theoretical Physics, Centre for Mathematical Sciences, University of Cambridge, Wilberfoce Road, Cambridge CB3 0WA*
[5]*Institute of Theoretical Astrophysics, University of Oslo, PO Box 1029 Blindern, 0315 Oslo, Norway*
[6]*Dipartimento di Fisica 'G. Galilei' universitá di Padova, INFN Sezione di Padova, via Marzolo 8, 1-35131 Padova, Italy*
[7]*INFN, Sezione di Padova, via Marzolo 8, I-35131, Padova, Italy*

Accepted 2008 July 2. Received 2008 June 19; in original form 2008 February 25

ABSTRACT

We present an analysis of the Minkowski Functionals (MFs) describing the *Wilkinson Microwave Anisotropy Probe* (*WMAP*) 3-yr temperature maps to place limits on possible levels of primordial non-Gaussianity. In particular, we apply perturbative formulae for the MFs to give constraints on the usual non-linear coupling constant $f_{\rm NL}$. The theoretical predictions are found to agree with the MFs of simulated cosmic microwave background (CMB) maps including the full effects of radiative transfer. The agreement is also very good even when the simulation maps include various observational artefacts, including the pixel window function, beam smearing, inhomogeneous noise and the survey mask. We accordingly find that these analytical formulae can be applied directly to observational measurements of $f_{\rm NL}$ without relying on non-Gaussian simulations. Considering the bin-to-bin covariance of the MFs in *WMAP* in a chi-square analysis, we find that the primordial non-Gaussianity parameter is constrained to lie in the range $-70 < f_{\rm NL} < 91$ [95 per cent confidence level (C.L.)] using the $Q + V + W$ co-added maps.

Key words: methods: analytical – methods: statistical – cosmic microwave background – early Universe.

1 INTRODUCTION

The existence of non-Gaussianity in primordial density fields has the potential to provide a unique observational probe that will enable discrimination among wide variety of inflationary models of the early Universe. Versions of the inflation scenario based on the idea of a single slow-rolling scalar field predict levels of non-Gaussianity too small to be observed. On the other hand, multi-field inflation models and models with a non-standard kinetic term for the inflation may yield larger non-Gaussian effects which could in principle be detected in current or next-generation observations (e.g. Bartolo, Matarrese & Riotto 2002; Bernardeau & Uzan 2002; Lyth, Ungarelli & Wands 2003; Alishahiha, Silverstein & Tong 2004; Arkami-Hamed et al. 2004; Bartolo et al. 2004; Dvali, Gruzinov & Zaldarriaga 2004; Battefeld & Battefeld 2007; Chen, Richard & Eugene 2007; Koyama et al. 2007).

In this paper, we focus on the local parametrization of primordial non-Gaussianity by including quadratic corrections to the curvature perturbation during the matter era (e.g. Komatsu & Spergel 2001):

$$\Phi = \phi + f_{\rm NL}(\phi^2 - \langle\phi^2\rangle), \tag{1}$$

where ϕ represents an auxiliary random-Gaussian field and $f_{\rm NL}$ characterizes the amplitude of the non-linear contribution to the overall perturbation. This local form is motivated by the simple slow-rolling single scalar inflation scenario and other models, including curvaton models (for an alternative parametrization of $f_{\rm NL}$, see Creminelli et al. 2007a). Current observations are not sufficiently sensitive to detect the wavelength dependence of $f_{\rm NL}$, so a constant $f_{\rm NL}$ provides a reasonable parametrization of the level of non-Gaussianity.

The analysis of the angular bi-spectrum for the *Wilkinson Microwave Anisotropy Probe* (*WMAP*) 3-yr data provides a constraint on $f_{\rm NL}$ to lie between -54 and 114 at the 95 per cent

★E-mail: chiaki.hikage@astro.cf.ac.uk

confidence level (C.L.) (Komatsu et al. 2003; Spergel et al. 2007). Creminelli et al. (2007a) obtain more stringent constraint $-36 < f_{\rm NL} < 100$. On the other hand, Yadav & Wandelt (2007) recently reported a detection of primordial non-Gaussianity at greater than 99.5 per cent significance. Further detailed analyses of non-Gaussianity are clearly necessary in order to reconcile and understand the various constraints and claimed detections.

Different approaches to the study of non-Gaussianity exploit different statistical properties and will be sensitive to different aspects of the behaviour of the pattern being tested. In general, there is no unique statistic to describe the non-Gaussian nature of a sample in a complete manner. A given method may have strong discriminatory power for one particular form of non-Gaussianity, but this is not necessarily the case for all possible alternative distributions. Testing non-Gaussianity therefore requires a battery of complementary techniques rather than a single approach. It is particularly important to use different statistical approaches in the context of primordial non-Gaussianity, because the physical mechanism responsible remains unknown. Furthermore, in the real world, issues including survey masks and inhomogeneous noise have to be taken into consideration. Different statistics may be sensitive to different systematics and foreground artefacts, so that complementary analysis using different statistics is essential for a robust detection. Analyses using different statistical methods are useful to validate or refute basic theoretical models and constrain model parameters more accurately. The most commonly used statistic for non-Gaussian analysis is the bispectrum (or even trispectrum) which focuses on information contained within three-point (or four-point) correlations. Other approaches represented by Minkowski Functionals (MFs) and genus statistics (one of MFs) utilize information concerning the integrated morphology and topology of the density structure, and are dependent on all order of correlation functions. Their robustness and generality therefore make them ideal complements to standard correlation analyses.

In this analysis, we focus on the *local* model of primordial non-Gaussianity characterized by $f_{\rm NL}$ in equation (1). Creminelli, Senatore & Zaldarriaga (2007b) show that the bispectrum is the optimal statistics in the estimation of $f_{\rm NL}$ and then other statistics (e.g. trispectrum) are useless even if there are different foreground contaminations. This is, however, only the case when the local model exactly describes the real universe. Other forms of non-Gaussianity, different from the one purely characterized by $f_{\rm NL}$, which may exist in a real observation, could make the fit of the theoretical estimation as a function of $f_{\rm NL}$ to the observation worse and also influence the estimation of $f_{\rm NL}$ among different statistics. Different statistical approaches are, therefore, still useful to test the assumed model of primordial non-Gaussianity and also possible observational systematics by checking if they have a reasonable goodness of the fit to observations and thus give a consistent limit on $f_{\rm NL}$ compared to that from the bispectrum.

In this paper, we present a measurement of primordial non-Gaussianity from the MFs of the *WMAP* 3-yr temperature maps. We apply perturbative formulae recently derived by Hikage, Komatsu & Matsubara (2006) to do the comparison with observations; previous analyses rely on non-Gaussian simulations (Komatsu et al. 2003; Spergel et al. 2007). The agreement of the theoretical predictions with non-Gaussian simulations has already been established in the Sachs–Wolfe limit (Hikage et al. 2006). In this paper, we apply non-Gaussian simulations based on full radiative transfer computations and then demonstrate that the analytical predictions accurately reproduce the simulation results. Gott et al. (2007) already derived an analytical formula for the genus statistic in the Sachs–Wolfe approximation to compare with *WMAP* data. Our analysis takes more detailed physics into account and is consequently more accurately applicable to a wider range of scales.

Observational effects (including antenna beam pattern, inhomogeneous noise and the survey mask) could be other sources of confusion. From a comparison with simulations including these observational issues, we find that the observational systematics are negligible to estimate the primordial non-Gaussianity from *WMAP* data directly using our method.

This paper is organized as follows. In Section 2, the *WMAP* 3-yr data studied here are briefly introduced. In Section 3, we test whether the perturbative formulae well describe the MFs for the non-Gaussian simulation maps even including the various observational effects mentioned above. In Section 4, we show the MFs for *WMAP* 3-yr temperature maps compared with theoretical formulae and give constraints on $f_{\rm NL}$. Section 5 is devoted to a summary and the conclusions.

2 *WMAP* 3-YR DATA

The cosmic microwave background (CMB) temperature maps derived from the *WMAP* observation are pixelized in HEALPix format with the total number of pixels $n_{\rm pix} = 12N_{\rm side}^2$ (Górski et al. 2005). In our analysis, we use the maps for Q, V and W frequency bands with $N_{\rm side} = 512$. The linearly co-added maps are constructed using an inverse weight of the pixel-noise variance $\sigma_0^2/\bar{N}_{\rm obs}$, where σ_0 denotes the pixel noise for each differential assembly (DA) given in Bennett et al. (2003) and $\bar{N}_{\rm obs}$ represents the full-sky average of the effective number of observations per each pixel. We adopt two maps with different combinations of frequency bands: V and W (written as '$V + W$') and Q, V and W (written as '$Q + V + W$'). The co-added maps are masked with the *Kp0* galaxy mask including point-source mask provided by Bennett et al. (2003), which leaves 76.8 per cent of the sky available for the data analysis.

In comparison with *WMAP* observations to give constraint on $f_{\rm NL}$ in Section 4, a Λ cold dark matter (CDM) cosmology is assumed with the cosmological parameters at the maximum likelihood peak from the *WMAP* 3-yr data only fit (Spergel et al. 2007): $\Omega_{\rm b} = 0.04309, \Omega_{\rm CDM} = 0.211, \Omega_\Lambda = 0.74591, H_0 = 71.227\,{\rm km\,s^{-1}\,Mpc^{-1}}, \tau = 0.08982$ and $n_{\rm s} = 0.95537$. The amplitude of the primordial fluctuations has been normalized by the first acoustic peak of the temperature power spectrum, $l(l+1)C_l/(2\pi) = 5617.05(\mu{\rm K})^2$ at $l = 220$ (Hinshaw et al. 2007).

3 PERTURBATIVE FORMULAE VERSUS NON-GAUSSIAN SIMULATIONS

3.1 Perturbative formulae of MFs for CMB with primordial non-Gaussianity

The topology of random fluctuation fields is generally studied using their excursion sets, i.e. regions where the field exceeds some threshold level. In a two-dimensional random field such as a CMB temperature map, three MFs are defined: the fraction of area V_0 exceeding the threshold, the total circumference V_1 of all the entire excursion set and the corresponding Euler Characteristic V_2 (Coles 1988). We measure MFs for CMB temperature maps as a function of the threshold density ν, defined as the temperature fluctuation $\Delta T/T$ normalized by its standard deviation $\sigma_0 \equiv \langle(\Delta T/T)^2\rangle^{1/2}$. Based on the general formalism of perturbation theory for MFs

(Matsubara 2003), Hikage et al. (2006) derived perturbative formulae of the MFs as a function of the non-linear coupling parameter $f_{\rm NL}$ (equation 1).

The MFs are separately written with the amplitude and the function of ν as follows:

$$V_k(\nu) = A_k v_k(\nu). \tag{2}$$

The amplitude A_k, which is determined only by the angular power spectrum C_l, is given by

$$A_k = \frac{1}{(2\pi)^{(k+1)/2}} \frac{\omega_2}{\omega_{2-k}\omega_k} \left(\frac{\sigma_1}{\sqrt{2}\sigma_0}\right)^k, \tag{3}$$

$$\sigma_j^2 \equiv \frac{1}{4\pi} \sum_l (2l+1)\,[l(l+1)]^j\, C_l W_l^2, \tag{4}$$

where $\omega_k \equiv \pi^{k/2}/\Gamma(k/2+1)$ gives $\omega_0 = 1, \omega_1 = 2, \omega_2 = \pi$, and W_l represents the smoothing kernel determined by the pixel and beam window functions and any additional smoothing (e.g. a Gaussian kernel). In weakly non-Gaussian fields, the function $v_k(\nu)$ can be divided into the Gaussian term $v_k^{(\rm G)}$ and the non-Gaussian term at lowest order Δv_k:

$$v_k(\nu) = v_k^{(\rm G)}(\nu) + \Delta v_k(\nu, f_{\rm NL}). \tag{5}$$

Each term has the following form:

$$v_k^{(\rm G)} = e^{-\nu^2/2} H_{k-1}(\nu), \tag{6}$$

$$\Delta v_k(\nu, f_{\rm NL}) = e^{-\nu^2/2} \left\{ \left[\frac{1}{6} S^{(0)} H_{k+2}(\nu) + \frac{k}{3} S^{(1)} H_k(\nu) + \frac{k(k-1)}{6} S^{(2)} H_{k-2}(\nu) \right] \sigma_0 + \mathcal{O}(\sigma_0^2) \right\}, \tag{7}$$

where $H_n(\nu)$ represent the nth Hermite polynomials and the skewness parameters $S^{(k)}$ are given in equations (27–29) of Hikage et al. (2006). The amplitude A_k (equation 3) is not directly relevant to non-Gaussianity but is dependent on the shape of C_l. We therefore concentrate on the non-Gaussian term Δv_k hereafter. The quantity Δv_k is the same as the relative difference of MFs, which are plotted in fig. 2 in Hikage et al. (2006), except for its normalization factor; in this paper the difference of MFs is normalized by A_k (3), while the maximum value of MFs for Gaussian fields is used in Hikage et al. (2006).

3.2 Comparison with non-Gaussian simulations

The above analytical formulae have already been found to accurately match the MFs for non-Gaussian maps in the Sachs–Wolfe limit (appendix C in Hikage et al. 2006). Here, we test them against non-Gaussian simulations including the full radiative transfer function (Liguori, Matarrese & Moscardini 2003; Liguori et al. 2007). As we mentioned in the Introduction, actual observations of CMB also involve different effects that may produce other confusions: the pixel window function, beam smearing, the inhomogeneous noise, survey mask and so on. We include these observational effects into the simulations to check whether they could have a systematic effect on our topological measures.

The cosmology in the non-Gaussian simulations is based on ΛCDM, but the cosmological parameters have slightly different values from *WMAP* 3-yr best fit; $\Omega_{\rm b} = 0.05, \Omega_{\rm CDM} = 0.25, \Omega_\Lambda = 0.7, H_0 = 65\,{\rm km\,s^{-1}\,Mpc^{-1}}, \tau = 0$ and $n_{\rm s} = 1$. The amplitude of primordial fluctuations is, however, set to be the same as *WMAP* 3-yr best-fitting value $l(l+1)C_l/(2\pi) = 5617.05(\mu{\rm K})^2$.

Observational effects related to *WMAP* data are included as follows. First, we convolve the original simulation maps with the $Q+V+W$ co-added beam transfer function with inverse weight of the full-sky averaged pixel-noise variance in each DA. Next, we add independent Gaussian noise realizations following the noise pattern co-added with the same weight. The simulation map is then masked with the *Kp*0 galaxy mask. Finally, we smooth the simulation maps using a Gaussian filter with a smoothing scale of $\theta_{\rm s}$,

$$W_l = \exp\left[-\frac{1}{2} l(l+1)\theta_{\rm s}^2\right]. \tag{8}$$

The MFs are sensitive to the resolution (or smoothing) scale of a density field, and thereby we can obtain a variety of information from density fields using different levels of smoothing. The information extracted from varying smoothing scales is nevertheless limited because they are all derived from the same original field; the smoothed fields are not independent. Here we focus on the field smoothed by three different smoothing scales 10, 20 and 40 arcmin, where the limit on $f_{\rm NL}$ is sufficiently converged. To remove the effect of the survey mask near the boundary of the mask, we only use the pixels more than $2\theta_{\rm s}$ away from the boundary. The sky fraction used in the analysis for each smoothing scale is 41 per cent for $\theta_{\rm s} = 40$ arcmin, 62 per cent for $\theta_{\rm s} = 20$ arcmin and 73 per cent for $\theta_{\rm s} = 10$ arcmin.

The MFs for the measured CMB temperature anisotropy are computed from the integral of the curvature of iso-temperature contour lengths (the details are given in appendix A.1. of Hikage et al. 2006). The binning range of ν is set to be -3.6 to 3.6 with 18 equally spaced bins of ν per each MF. This binning way produces well-converged results irrespective of other choices of the range of ν and the number of bins.

We obtain the normalized MFs (equation 3) with the amplitude A_k computed from C_l of each realization. Then, the residuals of the normalized MFs from Gaussian predictions $\Delta\tilde{v}_\alpha$ are calculated at each bin of α, which denote a threshold value ν, a kind of MF k, and a smoothing scale parametrized with $\theta_{\rm s}$ or $N_{\rm side}$. Even when the MFs of Gaussian realizations are computed, however, the function $\Delta\tilde{v}_\alpha$ are not exactly equal to 0 due to the effect of pixelization, survey mask and other numerical artefacts. We therefore measure the deviations from the average of the measurements over Gaussian realizations and subtract them as

$$\Delta v_\alpha = \Delta\tilde{v}_\alpha - [\Delta\tilde{v}_\alpha]_{\rm Gaussian,mean}. \tag{9}$$

In Fig. 1, we compare the analytical predictions of variance, skewness and MFs with the measurements from the simulations for $f_{\rm NL} = 100$. The simulated results are the average over 200 realizations and the error bars represent the error for the average (the sample variance divided by the square root of 200). The averaged measurements for Gaussian CMB maps are subtracted from those for non-Gaussian maps in the simulated plots including variance and skewness as well as MFs (see equation 9). In the plots, we adopt the Gaussian maps which are generated from the same realizations of linear potential fields (ϕ in equation 1) as the non-Gaussian CMB maps. The sample variances, represented by the error bars, are cancelled very well in such plots so one can focus on the systematic effect of primordial non-Gaussianity. The analytical formulae are found to agree with the simulations extremely well even including all observational effects. This indicates that we can measure $f_{\rm NL}$

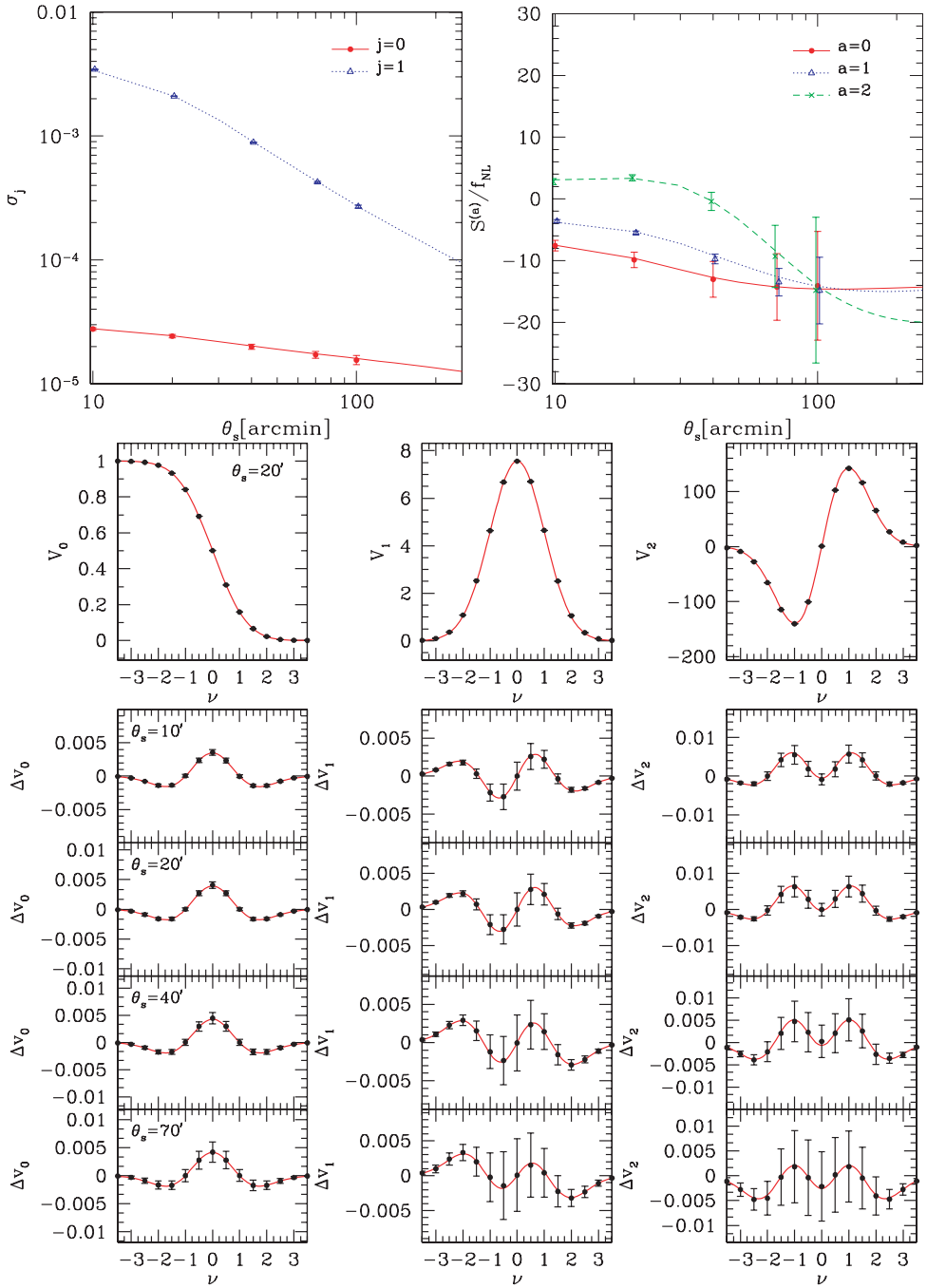

Figure 1. Comparison between the analytical predictions (lines) and the numerical estimations averaged over 200 realizations of non-Gaussian simulation maps (symbols) for $f_{\rm NL} = 100$. Upper-left: variances σ_0 and σ_1 (equation 4). Upper-right: skewness parameters $S^{(a)}$ ($a = 0$, 1 and 2) in the equation (7). Middle: MFs for non-Gaussian fields, V_k (equation 2). Lower: the difference ratio of MFs Δv_k (equation 7). CMB maps are smoothed with a Gaussian kernel $W_l = \exp\,[-\,l(l+1)\theta_s^2/2]$ where θ_s denotes the smoothing scale. The fully radiative transfer function is considered for both the theoretical predictions and the simulations. The simulations also include the various observational effects for *WMAP* 3-yr $Q + V + W$ co-added map; pixel window function, beam smearing, inhomogeneous noise pattern and *Kp0* cut. The error bars represent the errors for the averaged simulation results over 200 realizations (the sample variance divided by the square root of 200).

from direct comparison of the analytical formulae with observations without having to worry excessively about the presence of such systematics. We also check that both the artificial systematics $[\Delta\tilde{v}_\alpha]_{\rm Gaussian,mean}$ and covariance matrix are not strongly dependent on the details of cosmology. These results are encouraging, but not unexpected: being based on integrated properties, the MFs are expected to be robust to such effects.

4 CONSTRAINTS ON PRIMORDIAL NON-GAUSSIANITY FROM *WMAP* 3-YR DATA

4.1 Covariance matrix for MFs

We have adopted a maximum likelihood method to estimate the best-fitting value of $f_{\rm NL}$ and its associated uncertainty. In 'nearly

Gaussian' fields, the distribution functions of Δv_α are well described as multi-variate Gaussians. The likelihood function of $f_{\rm NL}$ is, therefore, simply proportional to $\exp(-\chi^2(f_{\rm NL})/2)$ where $\chi^2(f_{\rm NL})$ is computed using the theoretical formulae (equation 7) as

$$\chi^2(f_{\rm NL}) = \sum_{\alpha\alpha'} \left[\Delta v_\alpha^{\rm (obs)} - \Delta v_\alpha^{\rm (theory)}(f_{\rm NL})\right] \Sigma^{-1}_{\alpha\alpha'} \times \left[\Delta v_{\alpha'}^{\rm (obs)} - \Delta v_{\alpha'}^{\rm (theory)}(f_{\rm NL})\right], \quad (10)$$

where α and α' denote the binning number of threshold values ν, different kinds of MF k and smoothing scale parametrized with $\theta_{\rm s}$ or $N_{\rm side}$. The full covariance matrix $\Sigma_{\alpha\alpha'}$ is required because MFs are strongly correlated between different ν, different kinds of MF and also different $N_{\rm side}$ or $\theta_{\rm s}$. We estimate the covariance matrix of MFs from 1000 Gaussian simulation maps including the pixel and beam window function, *Kp0* survey mask and inhomogeneous noise for *WMAP* 3-yr maps.

The MFs contain information about fluctuations at different scales, so the results depend on the choice of window function. Here, two different types of window functions are adopted (in addition to the beam window functions). One is a Gaussian window function with the scale characterized by $\theta_{\rm s}$ (which is chosen to be sufficiently large compared with the pixel size). The other is just the pixel window function in HEALPIX format with a scale characterized by $N_{\rm side}$. The multi-pole components with l higher than $2N_{\rm side}$ are cut because they suffer from serious aliasing effects.

Before applying these ideas to the observational data, we check if our method based on χ^2 analysis is valid using simulations with primordial non-Gaussianity. We apply the non-Gaussian simulations to check that the likelihood function using equation (10) reproduces a valid probability distribution of the true value $f_{\rm NL}^{\rm (true)}$. Here, we consider that the likelihood function of $f_{\rm NL}^{\rm (true)}$ in each realization follows a Gaussian distribution around the best-fitting value $f_{\rm NL}^{\rm (best)}$ as

$$P(f_{\rm NL}^{\rm (true)}|f_{\rm NL}^{\rm (best)}) = \frac{1}{\sqrt{2\pi}\sigma_{f_{\rm NL}}} \exp\left[-\frac{1}{2}\left(\frac{f_{\rm NL}^{\rm (true)} - f_{\rm NL}^{\rm (best)}}{\sigma_{f_{\rm NL}}}\right)^2\right] \quad (11)$$

$$\sigma_{f_{\rm NL}} = \left[\sum_{\alpha\alpha'} \frac{\partial V_\alpha}{\partial f_{\rm NL}} (\Sigma^{-1})_{\alpha\alpha'} \frac{\partial V_{\alpha'}}{\partial f_{\rm NL}}\right]^{-1/2}, \quad (12)$$

where the binning number α represents a threshold ν for kth MF at a given scale $N_{\rm side}$ (or $\theta_{\rm s}$ if the Gaussian smoothing is added) and the covariance matrix $\Sigma_{\alpha\alpha'}$ is numerically estimated from Gaussian simulations. The function $\partial V_\alpha/\partial f_{\rm NL}$ is independent of $f_{\rm NL}$ (see equation 7) and thus the uncertainty $\sigma_{f_{\rm NL}}$ is independent of $f_{\rm NL}$. According to Bayes' theorem, $f_{\rm NL}^{\rm (best)}$ should distribute around $f_{\rm NL}^{\rm (true)}$ in the same way:

$$P(f_{\rm NL}^{\rm (best)}|f_{\rm NL}^{\rm (true)}) = P(f_{\rm NL}^{\rm (true)}|f_{\rm NL}^{\rm (best)}). \quad (13)$$

We estimate the distribution function of $f_{\rm NL}^{\rm (best)}$ from 200 non-Gaussian CMB simulated maps at a given $f_{\rm NL}^{\rm (true)}$ and then compare with equation (11). The simulated maps include observational effects represented by pixel and beam window functions, noise and *Kp0* survey cut for *WMAP* 3-yr data. Fig. 2 shows the theoretical predictions of $P(f_{\rm NL}^{\rm (best)}\,|\,f_{\rm NL}^{\rm (true)})$ at $f_{\rm NL}^{\rm (true)} = 0$ (solid) and 100 (dotted). From the MFs for the combined maps at Gaussian smoothing scales $\theta_{\rm s} = 20$ and 10 arcmin where the uncertainty is $\sigma_{f_{\rm NL}} = 44$. The histograms show the distribution of $f_{\rm NL}^{\rm (best)}$ from 200 (non-)Gaussian realizations. The averages of the best-fitting values of $f_{\rm NL}$ from the simulations are, respectively, 0 ± 44 (for $f_{\rm NL}^{\rm (true)} = 0$) and 101 ± 46 (for $f_{\rm NL}^{\rm (true)} = 100$). The simulations reproduce the theoretical predictions of the likelihood function very well. Our method is thus well established to give constraints on $f_{\rm NL}$ from *WMAP* 3-yr map.

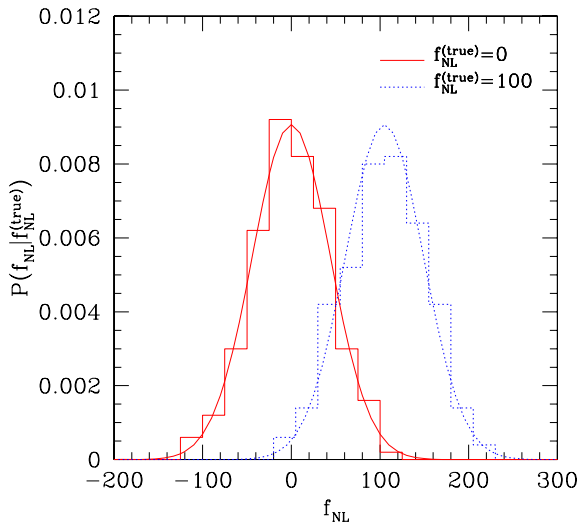

Figure 2. The distribution function of the best-fitting value of $f_{\rm NL}$ using *WMAP* 3-yr mock simulation maps (histogram). We use 200 realizations of Gaussian simulations (solid) and non-Gaussian simulations with $f_{\rm NL}^{\rm (true)} = 100$ (dotted), respectively. The best-fitting values are obtained by fitting the analytical formulae (equation 7) to all of the MFs for the simulations at $\theta_{\rm s} = 10$ and 20 arcmin combined. For comparison, we plot the likelihood function of $f_{\rm NL}$ at $f_{\rm NL}^{\rm (true)} = 0$ and 100 with $\sigma_{f_{\rm NL}} = 44$ (equation 11), which is the expected uncertainty of $f_{\rm NL}$ from all of the MFs for CMB maps at $\theta_{\rm s} = 10$ and 20 arcmin combined.

4.2 Constraints on $f_{\rm NL}$ from MFs for *WMAP* 3-Yr temperature anisotropy

The three MFs for the CMB temperature maps from *WMAP* 3-yr data are, respectively, plotted with symbols in each column of Fig. 3 (three left-hand columns for the '$Q + V + W$' map and three right-hand columns for the '$V + W$' map). In each column, the top panel shows the MF V_k at a representative scale ($\theta_{\rm s} = 20$ arcmin) and the lower three panels illustrate Δv_k at different $\theta_{\rm s} = 10, 20$ and 40 arcmin. The perturbative formulae with the best-fitting value of $f_{\rm NL}$ to each observed MF are plotted with lines. The best-fitting values and 1σ uncertainty are written in the left-bottom side of each panel. In top panels, all of the amplitude of observed MFs is found to be smaller than the theoretical estimations. This comes from the deficit of the observed power at low l which generates the larger amplitude of MFs determined by σ_1/σ_0 (equation 3), as pointed out by Gott et al. (2007). Fig. 4 shows the same plot but for the MFs with the pixel window function only. The top panel shows the MF at $N_{\rm side} = 128$ and the lower three panels illustrate Δv_k for $N_{\rm side} = 256$, 128 and 64. It is interesting that all MFs at $N_{\rm side} = 64$ have large positive values of $f_{\rm NL}$, though the significance is less than 2σ.

Table 1 lists the best-fitting values and the 1σ uncertainty of $f_{\rm NL}$ for each MF and their combined values at different sets of Gaussian smoothing scales $\theta_{\rm s}$. The 1σ uncertainty of $f_{\rm NL}$ is estimated from the range of $f_{\rm NL}$ with $\Delta\chi^2 = \chi^2 - \chi^2_{\rm min} \leq 1$. The minimum of chi-square $\chi_{\rm min}$ and the goodness-of-fit $P_{\chi^2 > \chi^2_{\rm min}}$ are listed for each fit. The results for the pixel window function only are shown in Table 2. The goodness-of-fit values are reasonable for all the fits, which means that the simple form of the primordial non-Gaussianity (equation 1)

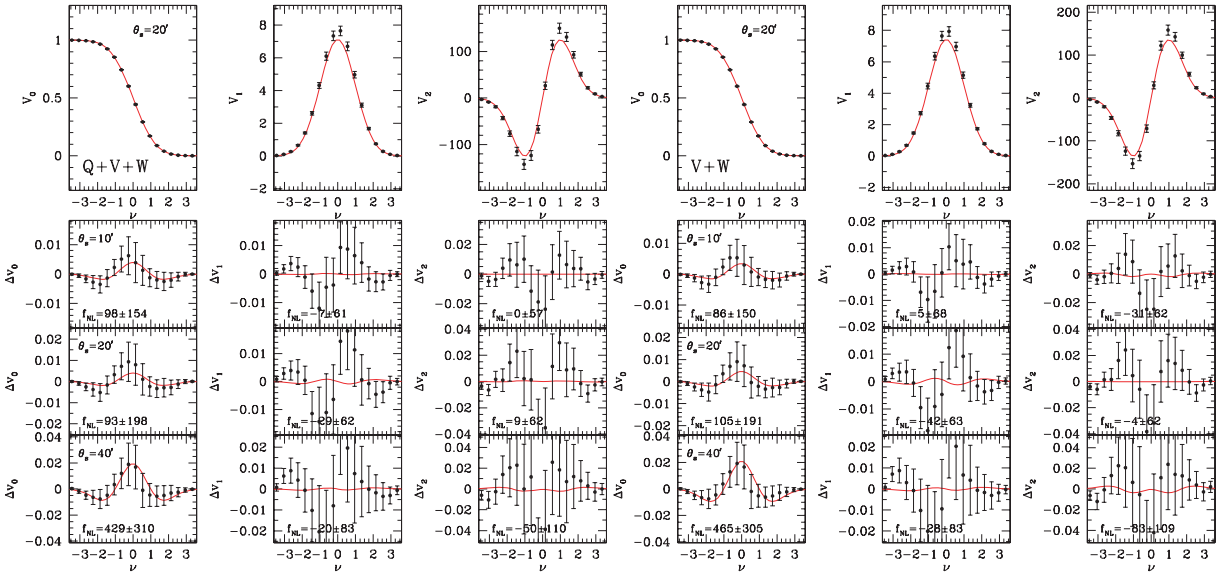

Figure 3. Comparison between MFs for *WMAP* 3-yr temperature maps (symbols) and the analytical formulae with the best-fitting value of $f_{\rm NL}$ for each MF (lines). The MFs are calculated from the $Q+V+W$ co-added map (left-hand side) and the $V+W$ map (right-hand side). Top panels show the MFs $V_k (k=0$, 1 and 2) at $\theta_{\rm s}=20$ arcmin, and other panels illustrate Δv_k (equation 7) at $\theta_{\rm s}=10$, 20 and 40 arcmin, respectively. Error bars denote the standard deviation of MFs at each bin of ν computed from 1000 Gaussian realizations including the *WMAP* 3-yr noise distribution, *Kp0* mask and pixel and beam window function. The systematics due to the pixelization effect are estimated from the Gaussian realizations and are subtracted from the observed MFs (see equation 9).

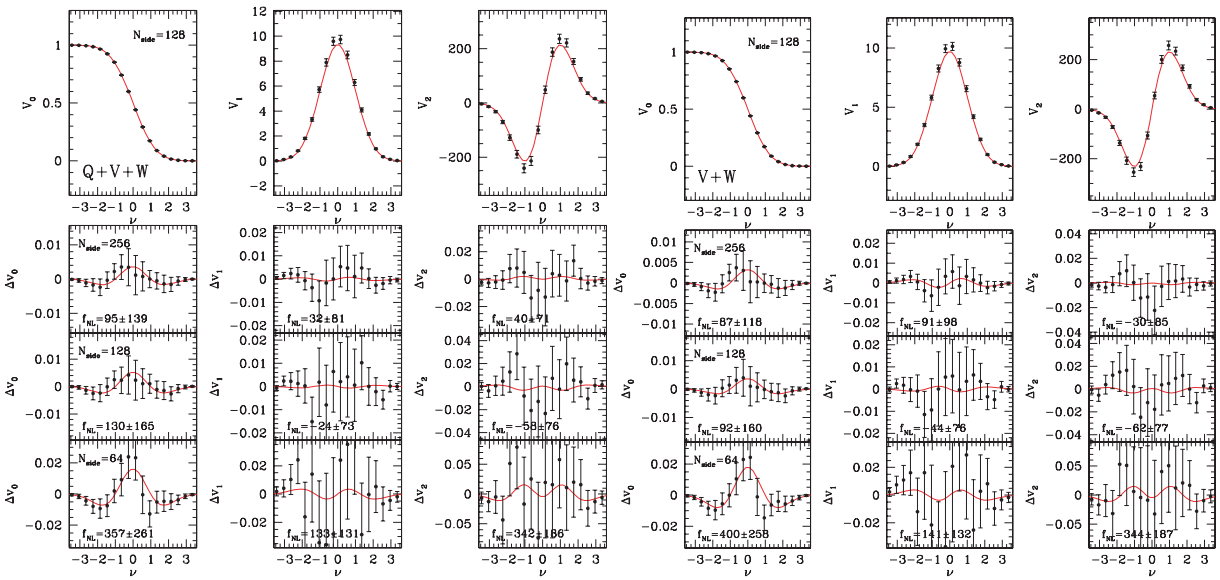

Figure 4. Same as Fig. 3 but for different $N_{\rm side}=256$, 128 and 64 without Gaussian smoothing.

well describes the behaviour of the observed MFs. In other words, present observations are too uncertain to allow the extraction of any further information about primordial non-Gaussianity (e.g. scale dependence of $f_{\rm NL}$). The constraint $-70 < f_{\rm NL} < 91$ at 95 per cent C.L. is obtained from all MFs for the $Q+V+W$ co-added map at combined different Gaussian smoothing scales of 10, 20 and 40 arcmin. A similar constraint is obtained from the MFs with pixel-window only as $-84 < f_{\rm NL} < 105$. The results from $Q+V+W$ co-added map are consistent with the previous ones (Creminelli et al. 2007a; Spergel et al. 2007).

There is some friction (but not disagreement) between our results and those by Yadav & Wandelt (2007); our $V+W$ analysis finds $f_{\rm NL}=-22\pm43$ whereas they find $f_{\rm NL}=87\pm30$. Moreover, our averaged $f_{\rm NL}$ decreases from $Q+V+W$ to $V+W$ whereas their $f_{\rm NL}$ increases. This is very interesting because there is the possibility that, for example, foregrounds and point sources might be biasing one of the two results. Yadav & Wandelt (2007) show in their analysis that these effects do not seem to contaminate the primordial bispectrum measurement significantly. It will be then important to check their effect on the MFs statistics in order to verify if this can explain the differences between the two results. However, the observed discrepancies already show how analysing non-Gaussianity using different statistics can provide additional interesting information.

Table 1. The constraints on $f_{\rm NL}$ from MFs for *WMAP* 3-yr co-added maps, $Q+V+W$ and $V+W$, at different Gaussian smoothing scales $\theta_{\rm s}$ (arcmin) of 40, 20 and 10 and their combination. For the calculation of their constraints, the maximum likelihood method is employed with the analytical formulae (equation 7) and the covariance matrix of MFs estimated from 1000 Gaussian realizations. The range of ν is set from −3.6 to 3.6 with the binning number per each MF of 18. The goodness-of-fit of the analytical formulae is represented by the minimum values of χ^2 value, $\chi^2_{\rm min}$, and the probability with χ^2 larger than $\chi^2_{\rm min}$.

			$Q+V+W$		$V+W$	
$\theta_{\rm s}$ (arcmin)	MF	d.o.f.	$\chi^2_{\rm min}(P_{\chi^2>\chi^2_{\rm min}})$	$f_{\rm NL}$	$\chi^2_{\rm min}(P_{\chi^2>\chi^2_{\rm min}})$	$f_{\rm NL}$
40	V_0	17	19.2 (0.32)	429 ± 310	23.7 (0.13)	465 ± 305
40	V_1	17	12.9 (0.75)	−20 ± 82	16.7 (0.48)	−28 ± 83
40	V_2	17	8.2 (0.96)	−50 ± 109	7.6 (0.97)	−83 ± 109
40	All	53	46.8 (0.71)	7 ± 76	48.8 (0.64)	−14 ± 77
20	V_0	17	20.8 (0.24)	93 ± 198	20.7 (0.24)	105 ± 191
20	V_1	17	14.0 (0.66)	−29 ± 62	12.6 (0.76)	−42 ± 63
20	V_2	17	13.9 (0.67)	9 ± 62	10.9 (0.86)	−4 ± 62
20	All	53	47.9 (0.67)	−32 ± 48	49.4 (0.61)	−53 ± 49
10	V_0	17	9.0 (0.94)	98 ± 154	9.4 (0.93)	86 ± 149
10	V_1	17	11.8 (0.81)	−7 ± 61	11.3 (0.84)	5 ± 67
10	V_2	17	9.9 (0.91)	0 ± 57	7.9 (0.97)	−31 ± 61
10	All	53	42.4 (0.85)	−10 ± 46	52.7 (0.48)	−25 ± 52
10, 20 & 40	V_0	53	49.0 (0.63)	8 ± 74	55.5 (0.38)	−20 ± 76
10, 20 & 40	V_1	53	41.4 (0.88)	−20 ± 55	44.2 (0.80)	−23 ± 57
10, 20 & 40	V_2	53	34.8 (0.98)	5 ± 52	28.3 (1.00)	−19 ± 53
10, 20 & 40	All	161	148.4 (0.75)	11 ± 40	173.2 (0.24)	−22 ± 43

Table 2. Same as Table 1 but for different $N_{\rm side}=64$, 128 and 256 without Gaussian smoothing.

			$Q+V+W$		$V+W$	
$N_{\rm side}$	MF	d.o.f.	$\chi^2_{\rm min}(P_{\chi^2>\chi^2_{\rm min}})$	$f_{\rm NL}$	$\chi^2_{\rm min}(P_{\chi^2>\chi^2_{\rm min}})$	$f_{\rm NL}$
64	V_0	17	17.5 (0.42)	357 ± 260	18.7 (0.34)	400 ± 257
64	V_1	17	18.7 (0.34)	133 ± 131	19.2 (0.32)	141 ± 132
64	V_2	17	12.2 (0.79)	342 ± 186	8.3 (0.96)	344 ± 187
64	All	53	46.9 (0.71)	137 ± 122	44.1 (0.80)	104 ± 123
128	V_0	17	25.0 (0.09)	130 ± 165	15.5 (0.56)	92 ± 160
128	V_1	17	25.5 (0.08)	−24 ± 73	19.7 (0.29)	−44 ± 76
128	V_2	17	14.1 (0.66)	−58 ± 76	16.5 (0.49)	−62 ± 77
128	All	53	55.8 (0.37)	−10 ± 60	41.6 (0.87)	−45 ± 62
256	V_0	17	7.2 (0.98)	95 ± 139	13.1 (0.73)	87 ± 118
256	V_1	17	8.7 (0.95)	32 ± 81	9.4 (0.93)	91 ± 98
256	V_2	17	10.1 (0.90)	40 ± 71	9.4 (0.93)	−30 ± 85
256	All	53	38.1 (0.94)	26 ± 60	41.0 (0.89)	−13 ± 69
256, 128 & 64	V_0	53	55.9 (0.37)	−44 ± 109	54.5 (0.42)	−21 ± 99
256, 128 & 64	V_1	53	61.4 (0.20)	−15 ± 63	55.2 (0.39)	−20 ± 67
256, 128 & 64	V_2	53	41.5 (0.87)	−7 ± 60	41.2 (0.88)	−51 ± 63
256, 128 &64	All	161	165.3 (0.39)	11 ± 47	152.4 (0.67)	−48 ± 48

5 SUMMARY AND CONCLUSIONS

We have presented an analysis of MFs for *WMAP* 3-yr temperature maps to limit the primordial non-Gaussianity characterized by the non-linear coupling parameter $f_{\rm NL}$. To do this, we compared perturbative formulae for MFs of weakly non-Gaussian fields directly with the observations. The analytical formulae are found to be in excellent agreement with results from non-Gaussian simulations of CMB maps including full radiative transfer effects. The agreement is still very good when including systematic observational effects including the *Kp0* survey mask, pixel and beam window functions, and inhomogeneous noise distribution for *WMAP* 3-yr data.

We have performed a χ^2 analysis to the comparison of the analytical formulae with *WMAP* 3-yr data. The fits of the analytical formulae to the observations are acceptable, and we thus obtain a robust constraint of $-70 < f_{\rm NL} < 91$ at 95 per cent C.L. from the $Q+V+W$ co-added maps with Gaussian filter at different scales 10, 20 and 40 arcmin combined. The result is consistent with previous results (Creminelli et al. 2007a; Spergel et al. 2007; Yadav & Wandelt 2007).

The behaviour of the results for the $V+W$ maps raises some interesting issues; our constraint is negatively shifted $-108 < f_{\rm NL} < 64$ while Yadav & Wandelt (2007) find a more positive range $27 < f_{\rm NL} < 147$. The difference between the two results should be clearer in the near future survey represented by *Planck*. It is worth investigating this result in further detail through a careful analysis of foregrounds and point source effects. This will be the subject of future work.

ACKNOWLEDGMENTS

We thank the anonymous referee for providing very useful comments and suggestions. We deeply appreciate Eiichiro Komatsu who originally proceeded with the project together. CH acknowledges support from the Particle Physics and Astronomy Research Council grant number PP/C501692/1. CH also acknowledges support from a Japan Society for the Promotion of Science (JSPS) fellowship. TM acknowledges the support from the Ministry of Education, Culture, Sports, Science and Technology, Grant-in-Aid for Scientific Research (C), 18540260, 2006 and Grant-in-Aid for Scientific Research on Priority Areas No. 467 'Probing the Dark Energy through an Extremely Wide & Deep Survey with Subaru Telescope'. SM acknowledges ASI contract Planck LFI Activity of Phase E2, for partial financial support.

REFERENCES

Alishahiha M., Silverstein E., Tong D., 2004, Phys. Rev. D., 70, 123505
Arkani-Hamed N., Creminelli P., Mukohyama S., Zaldarriaga M., 2004, J. Cosm. Astropart. Phys., 4, 1
Bartolo N., Matarrese S., Riotto A., 2002, Phys. Rev. D, 65, 103505
Bartolo N., Komatsu E., Matarrese S., Riotto A., 2004, Phys. Rept., 402, 103
Battefeld D., Battefeld T., 2007, JCAP, 5, 1
Bennett C. L. et al., 2003, ApJS, 148, 97
Bernardeau F., Uzan J.-P., 2002, Phys. Rev. D., 66, 103506
Chen X., Richard E., Eugene A. L., 2007, J. Cosm. Astropart. Phys., 6, 23
Coles P., 1988, MNRAS, 234, 509
Creminelli P., Senatore L., Zaldarriaga M., Tegmark M., 2006, J. Cosm. Astropart. Phys., 03, 005
Creminelli P., Senatore L., Zaldarriaga M., 2007, J. Cosm. Astropart. Phys., 03, 019
Dvali G., Gruzinov A., Zaldarriaga M., 2004, Phys. Rev. D., 69, 083505
Hikage C., Komatsu E., Matsubara T., 2006, ApJ, 653, 11
Górski K. M., Hivon E., Banday A. J., Wandelt B. D., Hansen F. K., Reinecke M., Bartelman M., 2005, ApJ, 622, 759
Gott J. R., III, Colley W. N., Park C. G., Park C., Mugnolo C., 2007, MNRAS, 377, 1668
Hinshaw G. et al., 2007, ApJS, 170, 288
Komatsu E., Spergel D. N., 2001, Phys. Rev. D, 63, 63002
Komatsu E. et al., 2003, ApJS, 148, 119
Koyama K., Mizuno S., Vernizzi F., Wands D., 2007, J. Cosm. Astropart. Phys., 11, 24
Liguori M., Matarrese S., Moscardini L., 2003, ApJ, 597, 57
Liguori M., Hansen F. K., Komatsu E., Matarrese S., Riotto A., 2006, Phys. Rev. D, 73, 043505
Liguori M., Yadav A., Hansen F. K., Komatsu E., Matarrese S., Wandelt B., 2007, Phys. Rev. D, 76, 105016
Lyth D. H., Ungarelli C., Wands D., 2003, Phys. Rev. D., 67, 23503
Matsubara T., 2003, ApJ, 584, 1
Spergel D. N. et al., 2007, ApJS, 170, 377
Yadav A. P. S., Wandelt B., D., 2007, Phys. Rev. Lett., 100, 181301

This paper has been typeset from a TEX/LATEX file prepared by the author.